http://dx.doi.org/10.5012/bkcs.2013.34.11.3367

Photoluminescence in MgO-ZnO Nanorods Enhanced by Hydrogen Plasma Treatment

Sunghoon Park, Hyunsung Ko, Youngho Mun, and Chongmu Lee*

*Department of Materials Science and Engineering, Inha University, Incheon 402-751, Korea. *E-mail: cmlee@inha.ac.kr*
Received August 9, 2013, Accepted August 28, 2013

MgO nanorods were fabricated by the thermal evaporation of Mg_3N_2. The influence of ZnO sheathing and hydrogen plasma exposure on the photoluminescence (PL) of the MgO nanorods was studied. PL measurements of the ZnO-sheathed MgO nanorods showed two main emission bands: the near band edge emission band centered at ~380 nm and the deep level emission band centered at ~590 nm both of which are characteristic of ZnO. The near band edge emission from the ZnO-sheathed MgO nanorods was enhanced with increasing the ZnO shell layer thickness. The near band edge emission from the ZnO-sheathed MgO nanorods appeared to be enhanced further by hydrogen plasma irradiation. The underlying mechanisms for the enhancement of the NBE emission from the MgO nanorods by ZnO sheathing and hydrogen plasma exposure are discussed.

Key Words : MgO nanorod, ZnO, Photoluminescence, Hydrogen plasma

Introduction

ZnO is one of a few materials that can emit short-wavelength light such as ultraviolet light and blue light. For the past decade, considerable efforts have been made to develop UV light-emitting devices based on ZnO, such as light-emitting diodes (LEDs) and lasers.[1-8] LEDs based on one-dimensional (1D) nanostructures have many advantages over thin film-based LEDs. Considerably improved performance is expected from nanostructured active layers for light emission. 1D nanostructures can act as direct waveguides and favor light extraction without the use of lens and reflectors. In addition, the emission efficiency is boosted by the absence of nonradiative recombinations at the joint defects because the use of 1D nanostructures can avoid grain boundaries.[9] Therefore, it is very important to obtain ultraintense short-wavelength luminescence using 1D nanostructures. Intense near-band edge (NBE) emission is obviously essential in the realization of high quality ultraviolet (UV) optoelectronic devices, such as LEDs and laser diodes (LDs). NBE emission is associated with the excitons bound to shallow donors, whereas deep level (DL) emission is associated with oxygen vacancy related defects, such as singly ionized oxygen vacancies, which can easily form recombination centers.[10-12]

A range of techniques have been used to enhance the NBE emission and simultaneously to suppress the DL emission of ZnO nanostructures. These techniques include thermal annealing in a hydrogen or oxygen atmosphere,[13] hydrogen or argon plasma treatment,[14] hydrogen or Ga doping,[15] and encapsulation of the nanostructures with thin films.[16] Of these techniques, formation of core-shell nanostructures by encapsulating ZnO nanostructures with other semiconducting oxide thin films has been reported by many research groups.[17-26] Recently, we reported that ultraintense short-wavelength emission could be obtained from ZnO-sheathed MgO nanorods induced by subwavelength optical resonance cavity formation.[27] This technique differs from previous encapsulation techniques in that the core and shell materials were MgO and ZnO, respectively. All the previous studies on encapsulation techniques used semiconducting oxide-sheathed ZnO nanostructures, *i.e.* ZnO-core/MgO-shell nanostructures to enhance the NBE emission and simultaneously to suppress the DL emission of ZnO nanostructures.

On the other hand, the improvement in the UV emission efficiency by hydrogen plasma exposure was reported by many research groups. ZnO usually shows strong green emission originating from deep levels caused by native oxygen vacancies.[28,29] It was recently found that the incorporation of hydrogen into ZnO could passivate the deep level green emission and enhance the near band edge UV emission efficiently.[30,31] The deep level emission caused by an oxygen vacancy is passivated by trapping hydrogen in the oxygen vacancy resulting in a hydrogen shallow donor bound in an oxygen vacancy as usually admitted.[32-34] This finding could benefit the development of many UV light-emitting devices based on ZnO. For instance, hydrogenation has lately been employed to enhance UV emission of the electroluminescence of n-ZnO/p-GaN LEDs.[35,36] In our previous paper on MgO-core/ZnO-shell nanowires we reported the effects of the ZnO shell layer thickness on the PL properties in the MgO-core/ZnO-shell nanowires. This study examined the effects of hydrogen plasma irradiation on the photoluminescence (PL) of the MgO-core/ZnO-shell nanowires. A combination of the two different techniques: a MgO-core/ZnO-shell nanostructure formation technique and a hydrogen plasma irradiation technique is expected to give a synergetic effect on the enhancement of the PL properties of ZnO.

Experimental

MgO nanorods were synthesized on Au-coated Si (100) substrates in a quartz tube by the thermal evaporation of Mg_3N_2. Details of the MgO nanorod synthesis procedure are

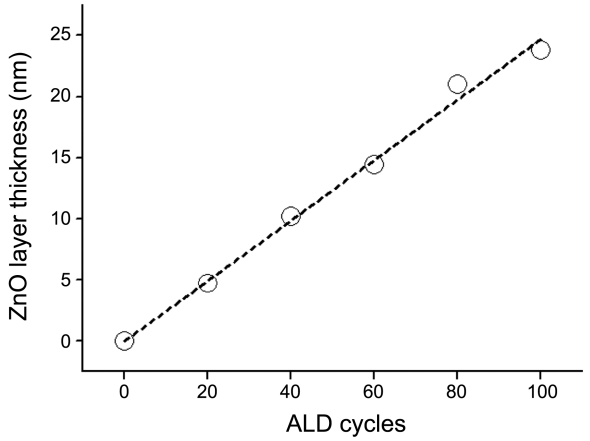

Figure 1. The ZnO shell layer thickness versus the number of ALD cycles.

described elsewhere.[37] The prepared MgO nanorods were then transferred to an atomic layer deposition (ALD) chamber. The ZnO was deposited on the nanorods using the following method. The nanorods were coated with ZnO. Diethylzinc (DEZn) and H_2O were kept in bubblers at 0° and 10 °C, respectively. These source gases were alternately fed into the chamber through separate inlet lines and nozzles. The typical pulse lengths were 0.15 sec for DEZn, 0.2 sec for H_2O and 3 sec to purge the reactants. The substrate temperature, pressure in the chamber, and base pressure were 150 °C, 0.1 Torr, and 2×10^{-6} Torr, respectively. The thickness of the ZnO shell layer formed by ALD appeared to be proportional to the number of ALD cycles as shown in Figure 1. Hydrogen plasma treatment was performed on the prepared pristine MgO nanorods and MgO/ZnO core-shell nanorods at room temperature for 1 min in a reactive ion etching (RIE) system (SAMCO, RIE-10NRU). The RIE system had a parallel-plate type plasma reactor and was operated at an RF frequency of 13.56 MHz. Hydrogen plasma was generated under the applied radio frequency (RF) power of 100 W, the gas flow of 100 sccm, and the pressure of 100 Pa.

The PL measurements of the nanorod samples were taken at room temperature using a PL spectrometer (SPEC-1403) with a He-Cd laser (325 nm, 55 mW) as the excitation source. The general surface morphology and crystallinity of the products were examined by scanning electron microscopy (SEM, Hitachi S-4200) and glancing angle (0.5°) X-ray diffraction (XRD, Rigaku DMAX 2500) with Cu-Kα radiation (λ = 0.1541 nm), respectively. A transmission electron microscope (TEM) instrument (Phillips CM-200) operated at 200 kV was used to examine the detailed microstructures of the products.

Results and Discussion

Figure 2(a) shows the SEM images of the MgO-core/ZnO-shell nanorods synthesized by the thermal evaporation of Mg_3N_2 powders at 900 °C for 1 h in an oxidizing atmosphere and the ALD of ZnO at 150 °C for 125 cycles. SEM observation of the core-shell nanorods revealed widths ranging from 80 to 120 nm and lengths ranging from 0.5 to 3 μm. The inset in Figure 2(a) clearly displays the geometrical configuration of a typical core-shell nanorod with faceted surfaces. Low-magnification TEM (Fig. 2(b)) revealed that the thickness uniformity of the ZnO shell layer formed on an MgO nanorod by ALD was not bad. The local high-resolution TEM image in Figure 2(c) shows the microstructures of the MgO core and the ZnO shell in a typical core-shell nanorod. The fringe pattern in the high-resolution TEM indicates the MgO core to be polycrystalline. The resolved spacing between two parallel neighboring fringes on the upper right side (Fig. 2(c)) was 0.24 nm, which matches well that of the {111} lattice plane family of face-centered cubic (fcc) (*Fm*3*m*)-structured MgO with a lattice parameter of a = 0.4213 nm (JCPDS No. 04-0829). A fringe pattern was also observed in the HRTEM of the shell region (Fig. 2(g)), indicating that the ZnO shell to also be of single crystal nature locally even though the overall structure of the ZnO shell is polycrystalline. The resolved spacing between two parallel neighboring fringes in the shell region was 0.25 nm, which is in good agreement with that of the {101} lattice plane family of an wurtzite (P63mc)-structured MgO with lattice parameters of a = 0.3253 nm and c = 0.5213 nm (JCPDS No. 89-1397). The corresponding selected area electron diffraction pattern recorded from the shell layer (Fig. 2(d)) clearly exhibited concentric ring patterns from the fcc-structured MgO and wurzite-structured ZnO, indicating both the MgO core and ZnO shell were polycrystalline. The reflections from the ZnO shell layer were weaker than those from the MgO core because the shell layer is thinner than the core.

The XRD pattern of the as-synthesized MgO-core/ZnO shell nanorods (Fig. 2(e)) showed that both the ZnO shells and MgO cores were crystalline. The (100), (002), (101), (110), and (103) reflection peaks of ZnO were observed alongside the strong (111), (200), and (220) reflection peaks of MgO. The heights of the ZnO reflection peaks were smaller than those of the MgO reflection peaks possibly because the ZnO shell layers were thinner than the MgO cores. The EDX spectrum taken from the core-shell nanorods (Fig. 2(f)) indicated the presence of Mg, Zn, and O elements, which agreed well with the result of XRD analysis (Fig. 2(e)). The Cu and C in the spectra are due to TEM grid. EDXS analyses confirmed that MgO/ZnO core-shell nanorods were synthesized successfully by showing the higher Mg concentration in the central region and the higher Zn Concentration at Both Edge Regions of the Nanorod (Fig. 2(g)).

Figure 3(a) shows the room-temperature PL spectra of the MgO-core/ZnO-shell nanorods for different numbers of ALD cycles for ZnO deposition. In the PL spectra, the as-synthesized MgO nanorods correspond to the 0 ALD cycle for ZnO deposition. The PL spectrum of the as-synthesized MgO nanorods showed a broad emission band centered at approximately 590 nm in the yellow region. In contrast, the MgO-core/ZnO-shell nanorods or the ZnO-sheathed MgO nanorods showed two characteristic emission bands: a sharp near-band edge emission band centered at approximately

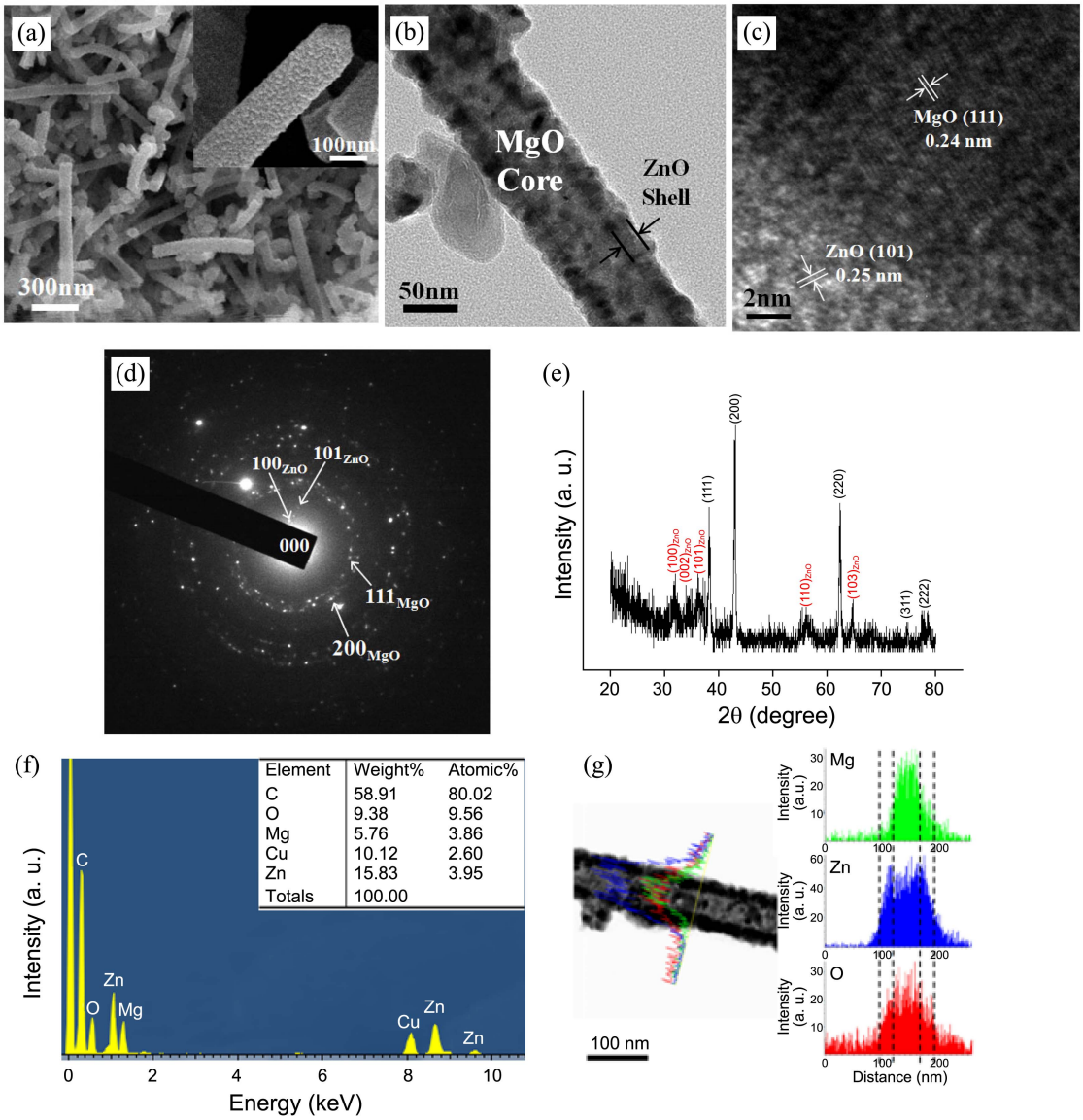

Figure 2. (a) SEM image of MgO/ZnO core-shell nanorods. Inset, enlarged SEM image of a typical MgO/ZnO core-shell nanorod. (b) Low-magnification TEM image of typical MgO/ZnO core-shell nanorods. (c) Local HRTEM image of typical MgO/ZnO core-shell nanorods near the core-shell interface. (d) Corresponding SAED pattern. (e) XRD pattern of the MgO/ZnO core-shell nanorods. (f) EDX spectrum of the MgO/ZnO core-shell nanorods. (g) EDXS concentration profile along the line drawn across the diameter of a typical MgO/ZnO core-shell nanorod.

380 nm in the near-ultraviolet region and a broad deep level emission band centered at 560 to 610 nm. These two bands are assumed to originate from the ZnO shell layer rather than from the MgO core because of the following two reasons: (1) The wavelengths of the two major emission peaks matched those of the near-band edge and deep level emissions from ZnO very well. (2) The peak height or the intensity of the emission increased with increasing the number of ALD cycles or the ZnO shell layer thickness. The ratio of the NBE emission intensity to the DL emission intensity (I_{NBE}/I_{DL}) as well as the ratio of the PL intensity of core-shell nanorods to that of the as-synthesized MgO nanorods (I/I_0) obviously increased with increasing the number of ALD cycles for ZnO deposition, as shown in Figure 3(b). The intensity ratio (I_{NBE}/I_{DL}) of the MgO-core/ZnO-shell nanorods for 100 cycles (corresponding to a ZnO shell layer thickness of ~25 nm) was ~2.15, whereas that of the pristine (unsheathed) MgO nanorods was 0. The NBE emission intensity ratio (I/I_0) of the MgO-core/ZnO-shell nanorods for 100 cycles to the core-shell nanorods for 0 cycles, *i.e.*, the pristine MgO nanorods was ~1.9 fold higher. Increasing the ZnO shell layer thickness resulted in an increase in the intensity ratio of the NBE emission to DL emission from the ZnO shell by enhancing the crystal quality of the ZnO thin film. The DL emission intensity decreased with increasing the ZnO shell layer thickness. In general, a thinner film contains a higher density of crystallographic defects such as surface states, vacancies, and dislocations than a thicker film because of a higher surface-to-volume ratio.

Here, it is worthy of noting that an MgO-core/ZnO-shell

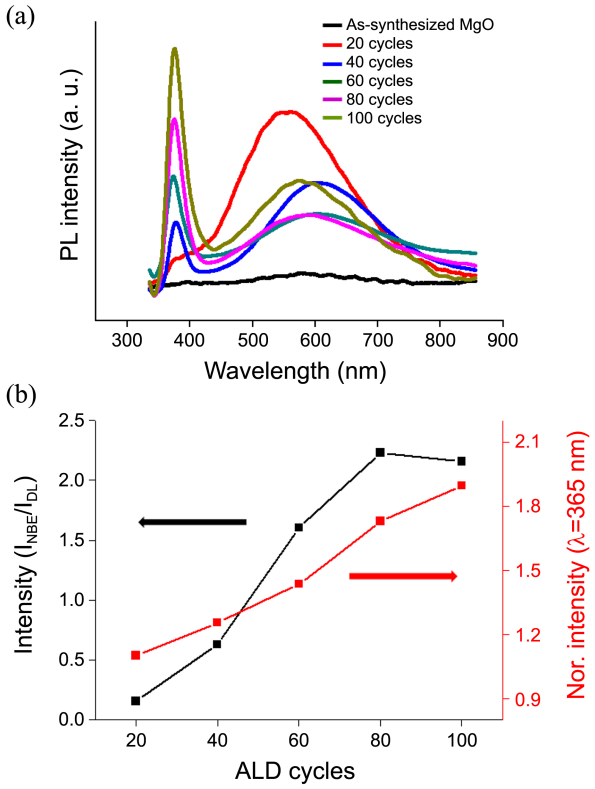

Figure 3. Room temperature-PL spectra of the as-synthesized MgO-core/ZnO-shell nanorods for different numbers of ALD cycles for ZnO deposition. (b) Plots of the intensity ratio of the NBE emission to the DL emission (I_{NBE}/I_{DL}) and the normalized intensity of the major emission (I/I_0) of the core-shell nanorods as a function of the number of ALD cycles for ZnO deposition. The PL intensity (I) was normalized to that of 0 ALD cycle (I_0). I is the intensity of the NBE emission from MgO-core/ZnO-shell nanorods, whereas I_0 is that of the DL emission from the MgO nanorods.

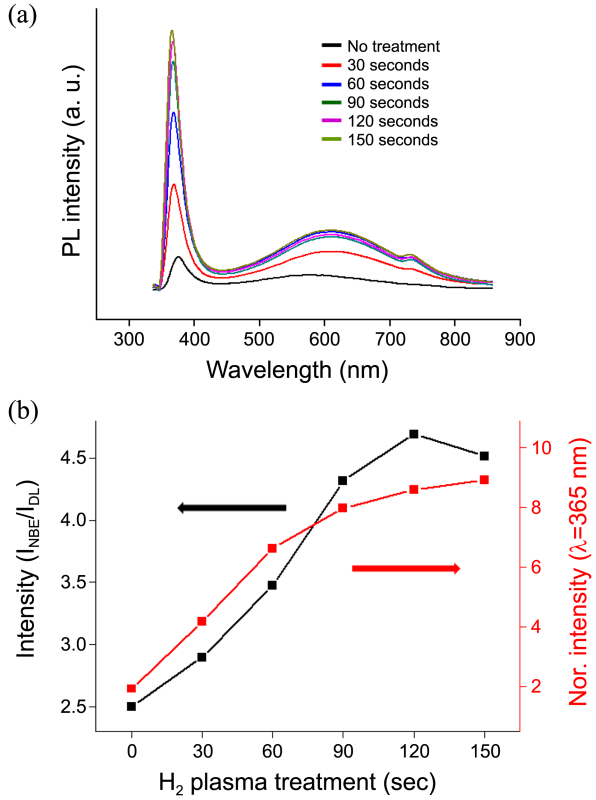

Figure 4. Room temperature-PL spectra of the as-synthesized MgO-core/ZnO-shell nanorods for different hydrogen plasma treatment times. (b) Plots of the intensity ratio of the NBE emission to the DL emission (I_{NBE}/I_{DL}) of the core-shell nanorods as a function of the hydrogen plasma treatment time.

nanorod is a more efficient nanomaterials than a simple ZnO nanorod in terms of the emission intensity, because the carrier transfer from the MgO core to the ZnO shell under laser illumination. It was hypothesized that some of these photogenerated electrons and holes recombine in the MgO cores to emit light, but that the remaining photogenerated electrons are transferred from the MgO cores to the ZnO shells. Unless the MgO nanorod surfaces were passivated with ZnO, the transferred photogenerated elesctrons would be readily captured by the defects at surfaces owing to the high specific surface area and short relaxation time for electrons tunneling from the inner parts of the MgO nanorods to the surfaces.[38,39] The transferring carriers are only electrons because holes do not transfer from MgO to ZnO due to the valence band edge (E_V) of MgO higher by 0.65 eV than that of ZnO.[40] In addition, MgO has unique properties such as an extraordinarily high secondary electron emission rate due to its negative electron affinity,[41] which may also have a positive effect on the transfer of the photogenerated electrons. On the other hand, the photogeneration of carriers in the ZnO shells is mainly caused by the band-to-band transition upon irradiation with a laser that has energy larger than the energy band gap (E_g) of ZnO. Next, the electrons and holes photogenerated in the ZnO shells and the electrons transferred from the MgO cores to ZnO shells recombine.

Figure 4(a) shows the effect of hydrogen plasma treatment on the PL properties of MgO-core/ZnO-shell nanorods. The intensity ratio of near-band edge emission to deep level emission, I_{NBE}/I_{DL}, tended to increase with increasing the plasma treatment time as shown in Figure 4(b). The I_{NBE}/I_{DL} of the MgO-core/ZnO-shell nanorods was ~4.8 for a plasma treatment time of 120 sec, whereas that of the pristine MgO nanorods was 0.

Both the NBE emission and DL emission peaks increased with increasing hydrogen plasma treatment, but the former increased much faster than the latter. This result is consistent with previous results in that the intensity ratio I_{NBE}/I_{DL} was increased by hydrogen plasma treatment. On the other hand, this result somewhat differs from a previous report that the DL emission peak was decreased while the NBE emission peak was increased by hydrogen plasma treatment.[42] As mentioned above, the DL emission from ZnO originates from the oxygen vacancies in ZnO.[10-12] The as-prepared core-shell nanorods contain a high density of oxygen vacancies. During H_2-plasma treatment, the oxygen vacancies are occupied by hydrogen atoms, leading to a decrease in DL emission and the enhancement in NBE emission. However, passivation of oxygen vacancies by hydrogen atoms can explain the decrease in the DL emission intensity but cannot

fully explain the increase in the NBE emission intensity.

For more qualitative explanation of the enhancement in the NBE emission of the core-shell nanorods with increasing plasma treatment time, at least four transition channels in ZnO including band-to-band, free-exciton, bound-exciton, and impurity-to band transitions should be taken into consideration. At room temperature, bound excitons completely dissociate due to their low binding energy typically 10-15 meV, and the fraction of the free-exciton transition increases. After the hydrogen plasma treatment, incorporation of hydrogen increases the free carrier concentration as well as introduces new donor levels. This should lead to an additional recombination channel via these donor centers resulting in the enhanced NBE emission. In addition, an increase in the free-carrier concentration should also lead to a strengthening of scattering processes which may further contribute to the more enhanced NBE emission of the treated samples.[43]

Conclusions

MgO/ZnO core-shell nanorods were synthesized on Si substrates using a two-step process: thermal evaporation of Mg_3N_2 and ALD of ZnO. PL measurements of the ZnO-sheathed MgO nanorods showed two main emission bands: the near band edge emission band centered at ~380 nm and the deep level emission band centered at ~590 nm both of which are characteristic of ZnO. The near band edge emission from the ZnO-sheathed MgO nanorods was enhanced with increasing the ZnO shell layer thickness. The near band edge emission from the ZnO-sheathed MgO nanorods was enhanced further by hydrogen plasma irradiation. The intensity ratio I_{NBE}/I_{DL} of the MgO/ZnO core-shell nanorods was increased with increasing the hydrogen plasma treatment time. The increase in I_{NBE}/I_{DL} is due to the passivation of oxygen vacancies by hydrogen atoms and the increase in the fraction of the free-exciton transition as results of the hydrogen plasma treatment.

Acknowledgments. This work was supported by the Key Research Institute Program' through the National Research Foundation of Korea (NRF) funded by the Ministry of Education, Science and Technology (2011-0018394).

References

1. Willander, M.; Nur, O.; Zhao, Q. X.; Yang, L. L.; Lorenz, M.; Cao, B. Q.; Zuñiga Perez, J.; Czekalla, C.; Zimmermann, G.; Grundmann, M.; Bakin, A.; Behrends, A.; Al-Suleiman, M.; El-Shaer, A.; Che Mofor, A.; Postels, B.; Waag, A.; Boukos, N.; Travlos, A.; Kwack, H. S.; Guinard, J.; Le Si Dang, D. *Nanotechnol.* **2009**, *20*, 332001.
2. Choi, Y. S.; Kang, J. W.; Hwang, D. K.; Park, S. J. *IEEE Trans. Electron Devices* **2010**, *57*, 26.
3. Park, W.I.; Yi, G. C. *Adv. Mater.* **2004**, *16*, 87.
4. Lai, E.; Kim, W.; Yang, P. *Nano Res.* **2008**, *1*, 123.
5. Zimmler, M. A.; Stichtenoth, D.; Ronning, C.; Yi, W.; Narayanamurti, V.; Voss, T.; Capasso, F. *Nano Lett.* **2008**, *8*, 16955.
6. Zimmler, M. A.; Bao, J.; Capasso, F.; Muller, S.; Ronning, C. *Appl. Phys. Lett.* **2008**, *93*, 051101.
7. Chen, M. T.; Lu, M. P.; Wu, Y. J.; Song, J.; Lee, C. Y.; Lu, M. Y.; Chang, Y. C.; Chou, L. J.; Wang, Z. L.; Chen, L. J. *Nano Lett*. **2010**, *10*, 4387.
8. Zimmler, M. A.; Voss, T.; Ronning, C.; Capasso, F. *Appl. Phys. Lett.* **2009**, *94*, 241120.
9. Lupan, O.; Pauporte, T.; Viana, B. *Adv. Mater.* **2010**, *22*, 3298.
10. Service, R. F. *Science* **1997**, *276*, 895.
11. Kang, H. S.; Kang, J. S.; Kim, J. W.; Lee, S. Y. *J. Appl. Phys*. **2004**, *95*, 1246.
12. van Dijken, A.; Meulenkamp, E. A.; Vanmaekelbergh, D.; Meijerink, A. *J. Lumin.* **2000**, *87-90*, 454.
13. Park, K. S.; Choi, Y. J.; Ahn, M. W.; Kim, D. W.; Sung, Y. M.; Park, J. G.; Choi, K. J. *J. Nanosci. Nanotechnol.* **2009**, *9*, 4328.
14. Li, Y.; Uchino, R.; Tokizono, T.; Paulsen, A.; Zhong, M.; Shuzo, M.; Yamada, I.; Delaunay, J. J. *Mater. Res. Soc. Symp. Proc.* **2010**, *1206*, M13-03.
15. Ohashi, N.; Isigaki, T.; Okada, N.; Sekifuchi, T.; Sakaguchi, I.; Haneda, H. *Appl. Phys. Lett*. **2002**, *80*, 2869.
16. Therry, R.; Perillat-Merceroz, G.; Jouneau, P. H.; Ferret, P.; Feuillet, G. *Nanotechnology* **2012**, *23*, 085705.
17. Kuang, Q.; Jiang, Z. Y.; Xie, Z. X.; Lin, S. C.; Lin, Z. W.; Xie, S. Y.; Huang, R. B.; Zheng, L. S. *J. Am. Chem. Soc*. **2005**, *127*, 11777.
18. Yu, D. W.; Li, X. M.; Gao, X. D. *Nanotechnology* **2005**, *16*, 2770.
19. Shi, L.; Xu, Y.; Hark, S.; Liu, Y.; Wang, S.; Peng, L.; Wong, K.; Li, Q. *Nano Lett*. **2007**, *7*, 3559.
20. Lin, C. C.; Chen, Y. W.; Chiang, M. C.; Lee, C. H.; Tung, Y. L.; Chen, S. Y. *J. Electrochem. Soc*. **2010**, *157*, H227.
21. Li, J.; Zhao, D.; Meng, X.; Zhang, Z.; Zhang, J.; Shen, D.; Lu, Y.; Fan, X. *J. Phys. Chem. B* **2006**, *110*, 14685.
22. Murphy, M. W.; Zhou, X. T.; Ko, J. Y. P.; Zhou, J. G.; Heigl, F.; Sham, T. K. *J. Chem. Phys*. **2009**, *130*, 084707.
23. Fu, Z.; Dong, W.; Yang, B.; Wang, Z.; Yang, Y.; Yan, H.; Zhang, S.; Zuo, J.; Ma, M.; Liu, X. *Solid State Commun*. **2006**, *138*, 179.
24. Shimpi, P.; Gao, P. X.; Goberman, D. G.; Ding, Y. *Nanotechnology* **2009**, *20*, 125608.
25. Plank, N. O. V.; Snaith, H. J.; Ducati, C.; Bendall, J. S.; Schmidt Mende, I.; Welland, M. E. A. *Nanotechnology* **2008**, *19*, 465603.
26. Chen, R.; Ye, Q. L.; He, T.; Ta, V. D.; Ying, Y.; Tay, Y. Y.; Wu, T.; Sun, H. *Nano Lett.* **2013**, *13*, 734.
27. Jin, C. H.; Kim, H. S.; Lee, C. *ACS Appl. Mater. Interfaces*. **2012**, *4*, 1262.
28. Richter, J.-P.; Voss, T.; Kim, D. S.; Scholz, R.; Zacharias, M. *Nanotechnology* **2008**, *19*, 305202.
29. Vanheusden, K.; Warren, W. L.; Seager, C. H.; Tallant, D. R.; Voigt, J. A.; Gnade, B. E. *J. Appl. Phys*. **1996**, *79*, 7983.
30. Vanheusden, K.; Seager, C. H.; Warren, W. L.; Tallant, D. R.; Voigt, J. A. *Appl. Phys. Lett*. **1996**, *68*, 403.
31. Sekiguchi, T.; Ohashi, N.; Terada, Y. *Japan. J. Appl. Phys*. **1997**, *36*, L289.
32. Ohashi, N.; Ishigaki, T.; Okada, N.; Taguchi, H.; Sakaguchi, I.; Hishita, S.; Sekiguchi, T.; Haneda, H. *J. Appl. Phys*. **2003**, *93*, 6386.
33. Lavrov, E.; Herklotz, F.; Weber, J. *Phys. Rev. Lett.* **2009**, *102*, 185502.
34. Lavrov, E. V. *Physica B* **2009**, *404*, 5075.
35. Lavrov, E. V.; Herklotz, F.; Weber, J. *Phys. Rev. B* **2009**, *79* 165205.
36. Fang, F.; Zhao, D.; Li, B.; Zhang, Z.; Shen, D. *Phys. Chem. Chem. Phys.* **2010**, *12*, 6759.
37. Zhang, S. G.; Zhang, X. W.; Zhang, J. X.; You, J. B.; Yin, Z. G.; Dong, J. J.; Cui, B.; Wowchak, A. M.; Dabiran, A. M.; Chow, P. P. *Phys. Status Solidi RRL* **2011**, *5*, 74.
38. Jin, C.; Kim, H.; Lee, W. I.; Lee, C. *Adv. Mater*. **2011**, *23*, 1982.
39. Guo, L.; Yang, S.; Yang, C.; Yu, P.; Wang, J.; Ge, W.; Wong, G. K. L. *Appl. Phys. Lett*. **2000**, *76*, 2901.
40. Bendre, B. S.; Mahamuni, S. *J. Mater. Res*. **2004**, *19*, 737.
41. Kim, H. K.; Kim, T. S.; Lee, J.; Jo, S. K. *Phys. Rev. B* **2007**, *76*, 165434.
42. Windisch, C. F.; Exarhos, G. J.; Yao, C. H.; Wang, L. Q. *J. Appl. Phys*. **2007**, *101*, 123711.